Universita di Trento
Dipartimento di Fisica
Trento, Italy

Charge Management in LISA Pathfinder: The Continuous Discharging Experiment

Author:
B.E. Ewing
Wright State University
Dayton, OH

Supervisor:
Dr. William Weber
Prof. Associato
Universita di Trento

August 2, 2017

Abstract

Test mass charging is a significant source of excess force and force noise in LISA Pathfinder (LPF). The planned design scheme for mitigation of charge induced force noise in LISA is a continuous discharge by UV light illumination. We report on analysis of a charge management experiment on-board LPF conducted during December, 2016. We discuss noise in the charge measurement taken with and without continuous UV illumination. We also give an exponential fit characterizing the behavior of the test mass charge under continuous UV illumination. Our results confirm the expectation that the continuous discharge scheme allows for lower net test mass charge with the trade-off of increased measurement noise.

Contents

1 Introduction

The report will begin with a short introduction giving the current standing of gravitational wave detection in the mHz frequency band, the LISA Pathfinder (LPF) experiment, and a description of the charge management problem. Section 2 presents the purpose and methodology behind a charge measurement experiment conducted onboard LPF in December 2016. Section 3 describes the derivations and methods used to calculate the Δg and charge time-series from LPF telemetry. Section 4 presents results of the various charging properties studied. Finally Section 5 is a discussion of these results in the context of the forthcoming LISA mission.

1.1 Background

Gravitational waves are emitted from diverse sources with frequencies spanning bands over many orders of magnitude. LIGO (Laser Interfermoter Gravitational-Wave Observatory) has already achieved unparalleled success in detecting gravitational waves in the frequency band of Hz to hundreds of Hz. Every signal that LIGO has detected to date has come from the inspiral and merger of binary black holes [1]. Although the LIGO detectors represent the standard of gravitational wave detection in the high frequency band, they are incapable of detecting gravitational waves in lower frequency bands. LISA (Laser Interferometer Space-Based Observatory) is a mission currently planned by ESA to detect gravitational waves in the mHz frequency band, where LIGO is insensitive.

There are many and diverse astrophysical sources emitting gravitational waves in the mHz frequency band. These include objects which are currently poorly understood by electromagnetic observations alone. The detection of mHz frequency gravitational waves from these sources will provide a new window into our universe.

The advantages of a space-based detector are immediately apparent in that it would not be subject to the same noise sources that dominate ground-based detectors in low frequencies. In space, it is also possible to surpass the spatial dimensions that limit ground-based detectors, allowing for increased sensitivity.

LISA will be the first gravitational wave detector in space. However, without prior testing and simulation, LISA would represent a major risk as an experiment. Considering the time and cost of building this detector and launching it into space it is imperative that LISA achieves results. It was largely for this reason that LISA Pathfinder (LPF), the science precursor mission to LISA, was implemented. With the resounding success and recent closure of the LPF mission, the next frontier of gravitational physics - the mHz frequency band - is one step closer.

1.2 LISA Pathfinder

LISA Pathfinder was designed to test the technology required by LISA. It was not designed to detect gravitational waves; instead, LPF tested scientific principles and modeled noise in the LISA detection band. LPF was in operation for about 16 months, carrying out various experiments controlled nearly in real-time by on-ground teams.

LISA Pathfinder was a single space craft which centered itself around two test masses as they traveled in a nearly perfect free-fall. It includes multiple subsystems for force shielding and data acquisition. While in operation, LPF orbited the first Sun-Earth Lagrange point (L1); the location was chosen for its thermal and gravitational stability, among other factors.

The LPF Technology Package (LTP) includes the gravitational reference system (GRS) and the optical metrology subsystem (OMS) [2]. The GRS protects the test masses from non-gravitational forces, while the OMS measures the positions of the test masses using multiple interferometers.

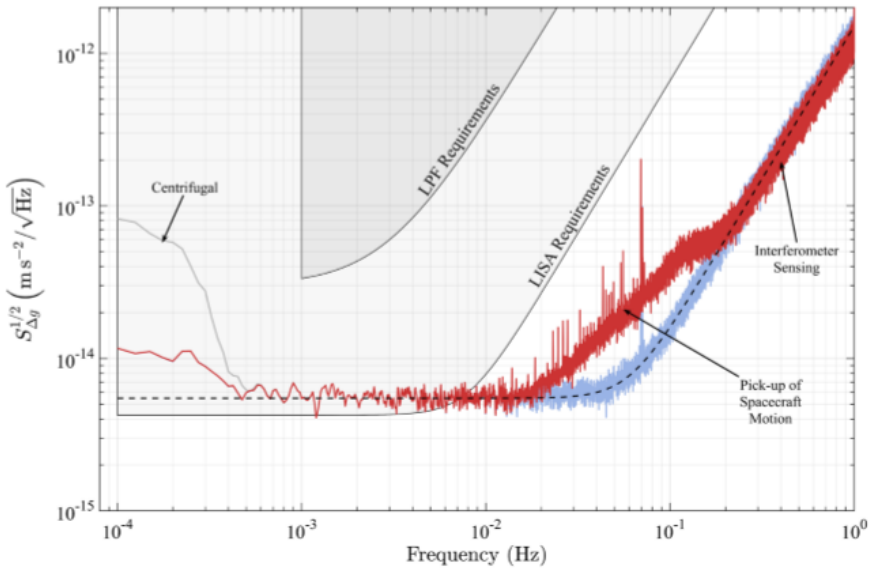

Figure 1: The plot shows the ASD of Δg from a 6.5 day noise-run near the beginning of the LPF mission launch. The shaded grey regions indicate the requirements for LPF and LISA. The grey curve shows the measured $S_{\Delta g}^{1/2}$; red and blue curves show $S_{\Delta g}^{1/2}$ after correction for some known noise sources. Reprinted from "Sub-Femto-g Free Fall for Space-Based Gravitational Wave Observatories: LISA Pathfinder Results", by M. Armano et al., 2016, *PRL*, 116(23), 231101-3. DOI: https://doi.org/10.1103/PhysRevLett.116.231101

The main goal of LPF was to demonstrate LISA's required level of sensitivity to the differential acceleration of the two test masses. The LPF requirement for the amplitude spectral density (ASD) of the differential acceleration, $S_{\Delta g}^{1/2}$ was $30 fms^{-2}Hz^{-1/2}$; this requirement was quickly met by LPF in the first days of its operation and represents the purest state of free-fall ever measured [3]. Figure 1 (reprinted from [3]) shows the ASD of Δg as measured from a noise-run near the beginning of the LPF mission. Beyond achieving this level of free-fall among the two test masses, LPF was also designed for experiments to characterize multiple noise sources on-board the spacecraft. This work will focus on characterizing charge-induced force noise.

1.3 Charge Management

The test masses were kept inside a vacuum enclosure and shielded by their respective electrode housings as well as the spacecraft itself, however, significant charging of the test masses still occurred. Incident cosmic rays and solar particles bombarded the test masses, depositing a net positive charge, building up over time. The charging rates were observed to be about $+22.9e/s$ and $+24.5e/s$ on TM1 and TM2 respectively [4]. This charging will occur in LISA as well, producing unwanted force and force noise acting on the test masses.

The Charge Management System (CMS), an element of the GRS, is designed to mitigate the effect of test mass charging. It is necessary that the CMS is able to maintain the charge on the test masses close to neutral while producing as little extra noise as possible. The CMS works on the principle of contact-free discharge by UV light illumination. Six mercury lamps on-board emit 235.7nm light incident on either the test masses themselves or their surrounding electrode housings [5]. Discharging occurs by the photoelectric effect; a current of electrons flowing between test mass and electrode housing is produced.

The forces due to the charge on each test

mass, F_1 and F_2, are obtained by modeling the test masses and their surrounding electrodes as a battery and a capacitor.

By this model, the total energy stored between the test mass and the electrodes is,

$$U = \frac{1}{2}CV^2 \tag{1}$$

Here, V is the potential difference between the electrodes and the test mass, $V = V_{EH} - V_{TM}$. V_{EH} is modeled by n 'patch voltages', each with its own voltage, V_i. Therefore, the potential difference between a single patch, and the entire test mass is $V_i - V_{TM}$ while the total potential difference, $V = \sum_i^n (V_i - V_{TM})$. Substituting this expression for V into Equation 1, and differentiating we obtain the force on one test mass,

$$F = \pm\frac{1}{2}\left|\frac{dC}{dx}\right|\sum_i^n (V_i - V_{TM})^2 \tag{2}$$

Here, absolute value bars are placed around $\frac{dC}{dx}$ since its sign depends on the position of the particular electrode being summed over. The voltage V_i can be expressed by the applied voltage to the electrode, $\pm V\sin(\omega t)$, where again the sign depends on the electrode being summed over [6]. Expanding the square in Equation 1 gives,

$$F = \pm\frac{1}{2}\left|\frac{dC}{dx}\right|\sum_i (\pm V\sin(\omega t))^2 + \sum_i (-V_{TM})^2 - 2\sum_i \pm V\sin(\omega t)V_{TM}$$

Expanding the first term out for all four electrodes gives,

$$\frac{1}{2}\left(+2\left|\frac{dC}{dx}\right| - 2\left|\frac{dC}{dx}\right|\right)\sum_i V^2\sin^2(\omega t) \tag{3}$$

which is obviously null, since all terms in the summation are positive. The same is true for the second term. Therefore the final term in Equation 3 is the only nonzero term. Expanding this out over the four electrodes gives,

$$F = -\frac{1}{2}\left(+2\left|\frac{dC}{dx}\right|\right)\sum_i +2V\sin(\omega t)V_{TM} - \frac{1}{2}\left(-2\left|\frac{dC}{dx}\right|\right)\sum_1 -2V\sin(\omega t)V_{TM}$$

$$F = -4\left|\frac{dC}{dx}\right| V\sin(\omega t)V_{TM} \tag{4}$$

This is the force due to charge acting on each test mass [6]. V_{TM} can be expressed in terms of the test mass charge as, $V_{TM} = q/C_{tot}$. So that equation 4 becomes,

$$F = -4\left|\frac{dC}{dx}\right| V\sin(\omega t)\frac{q}{C_{tot}} \tag{5}$$

Any noise in the charge, δq, or the charging rate, $\delta\Delta q$ would produce noise in F. A combination of charge value as close to neutral as possible and low charging noise would produce the smallest contribution from this force.

2 The Experiment

In December 2016 a charge measurement experiment was carried out on LISA Pathfinder. The experiment lasted for five days: December 13th - December 18th. The time was split into two principle investigations: a period of time with no UV discharging, allowing the test masses to accumulate charge followed by a period of continuous UV illumination and discharging.

2.1 Purpose

Test mass charging is a significant source of noise for LPF and in the future, LISA. While other sources of noise may be minimized by design before launch, test mass charging is inevitable and requires mitigation procedures onboard. The test masses must be discharged otherwise the noise due to charge related forces would quickly begin to dominate the signal. The chosen method of discharge is by UV illumination, primarily because it is contact-free. The immediate question is whether discharging should be continuous or periodic. It is expected that the

continuous discharging scheme would allow for the test mass charge to constantly remain near neutral, with the trade-off of added noise [4].

It is desirable to understand the noise that a continuous UV discharging scheme would contribute to measurement of Δg. The charge time series will exhibit different properties under continuous discharge as opposed to being allowed to accumulate charge during measurements. It's important to understand the properties of this charging behavior for use in LISA. By observing the test masses in back-to-back periods of charge accumulation and continuous discharging, these questions can be addressed.

2.2 Methodology

Investigation 1: 12/12 09:00 - 12/15 09:00
$V_{x1,TM1} = .1\sin((2\pi \cdot .003)t) + .06$
$V_{x1,TM2} = .1\sin((2\pi \cdot .003)t)$
Investigation 2.1: 12/15 09:06 - 12/15 14:00
$V_{x1,TM1} = .1\sin((2\pi \cdot .001)t) + .06$
$V_{x1,TM2} = .1\sin((2\pi \cdot .003)t)$
$UV_{lamp1} = 200$
$UV_{lamp2} = 100$
Investigation 2.2: 12/15 14:11 - 12/18 02:40
$V_{x1,TM1} = .1\sin((2\pi \cdot .001)t) + .06$
$V_{x1,TM2} = .1\sin((2\pi \cdot .003)t)$
$UV_{lamp1} = 5$
$UV_{lamp2} = 8$

Table 1: Applied x1 electrode voltages and current of UV lamps

As previously mentioned, the experiment was carried out in December 2016, lasting a total of 4 days and 14 hours. Investigation 1 lasted for about 140,400 seconds and Investigation 2 lasted for the remaining 255,300 seconds. Sinusoidal voltages were applied to each test mass over the length of the experiment. To distinguish between signal from each test mass a different modulation frequency was used for each test mass. TM1 was injected with $f_{mod1} = 1mHz$ and TM2 with $f_{mod2} = 3mHz$. The applied voltages and the current of the UV lamps (if in-use) during each investigation are shown in Table 1. Here, Investigation 2 is split in two segments to clarify that initially there was a fast discharging period followed immediately by the slow continuous discharge.

3 Data Analysis

All data from LISA Pathfinder was obtained via the LTPDA Toolbox on Matlab. Analysis was carried out within this toolbox, for convenience and reproducibility of results. In the LTPDA Toolbox data is stored, depending on its type, as either an analysis object (*ao*) or a parameter estimation object (*pest*). These each contain information about the data they store; most importantly, units, errors, descriptions, names, and histories.

3.1 Calculation of Differential Acceleration

All of the constants needed to perform the calculation of the differential acceleration, Δg, were obtained directly from LISA Pathfinder, through telemetry. They were stored as analysis objects inside the LTPDA environment throughout the entire process of data analysis. The positions of the test masses, as well as their applied forces were also obtained from telemetry. A summary of all data from telemetry is given in Table 2

Symbol	**Description**	**Units**
x_1	TM1 position wrt spacecraft	m
x_{12}	Differential TM position	m
F_1	Applied force on TM1	$kg \cdot m \cdot s^{-2}$
F_2	Applied force on TM2	$kg \cdot m \cdot s^{-2}$
m	TM mass	kg
ω_2^2	Stiffness of TM2	s^{-2}
ω_{12}^2	Differential TM stiffness	s^{-2}
C_1	Calibration factor for F_2	
τ	C_1· Time delay	s

Table 2: Data and useful constants obtained from telemetry.

The force on each test mass is modeled using Hooke's Law. TM1 is modeled as a spring under simple harmonic motion, while TM2 includes a driving or applied force, F_{2c}. The controlled force on TM2 takes into account calibration of the circuitry and a time delay $F_{2c} = C_1 F_{applied}(t - \tau)$. Expanding this as a Taylor Series to first order,

$$F_{2c} = C_1(F_a(t) - \tau \frac{dF_a}{dt}(t)) \tag{6}$$

The term $\frac{dF_a}{dt}(t)$ is calculated using a numerical 3-point derivative built into the LTPDA Toolbox, and the constants C_1 and τ are obtained from telemetry.

The equations of motion for TM1 and TM2 respectively are,

$$F_1 \equiv m_1 \ddot{x_1} = -k_1 x_1 \tag{7}$$

$$F_2 \equiv m_2 \ddot{x_2} = -k_2 x_2 + F_{2c} \tag{8}$$

Dividing through by the masses, and introducing the constants ω_1^2 and ω_2^2 Equations 8 and 9 simplify to,

$$\frac{F_1}{m_1} = \ddot{x_1} = -\omega_1^2 x_1 \tag{9}$$

$$\frac{F_2}{m_2} = \ddot{x_2} = -\omega_2^2 x_2 + g_{2c} \tag{10}$$

where the constant, $g_{2c} \equiv \frac{F_{2c}}{m_2}$, is also introduced. The differential acceleration is defined as the difference in force per unit mass of the two test masses,

$$\Delta g = \frac{F_2}{m_2} - \frac{F_1}{m_1} \tag{11}$$

$$\Delta g = (\ddot{x_2} - \ddot{x_1}) + (\omega_2^2 x_2 - \omega_1^2 x_1) - g_{2c} \tag{12}$$

For further simplification, the constants $o_{12} \equiv x_2 - x_1$ and $\omega_{12}^2 \equiv \omega_2^2 - \omega_1^2$ are introduced. The final form of the differential acceleration is given by,

$$\Delta g = \ddot{x_{12}} + \omega_2^2 x_{12} + \omega_{12}^2 x_1 - g_{2c} \tag{13}$$

Verification of the algebra leading to the previous equation is left to the reader.

3.2 Calculation of Test Mass Charge

In the previous section, Δg was defined as the difference in force per unit mass of the two test masses. Equation 11 can be simplified by expressing the mass of each test mass by the single constant, m. That is,

$$m\Delta g = F_2 - F_1 \tag{14}$$

Therefore, the amplitude of Δg is proportional to the amplitude of the forces, giving

$$m\Delta g = -4 \left| \frac{dC}{dx} \right| V V_{TM} \tag{15}$$

The test mass voltage is expressed in terms of the charge as, $V_{TM} = \frac{q}{C_{tot}}$ where C_{tot} is the total capacitance between the test mass and all electrodes. Finally, we obtain the charge in terms of Δg,

$$q(t) = \frac{-m\Delta g C_{tot}}{4 \left| \frac{dC}{dx} \right| V} \tag{16}$$

Because the voltage applied to each test mass is proportional to sine it is expected that the Δg and $q(t)$ signals will also be proportional to sines. Δg can be decomposed into its in- and out-of-phase components: $\Delta g_{\sin(\omega_1)}$ and $\Delta g_{\cos(\omega_1)}$ due to the voltage applied to TM1, and similarly, $\Delta g_{\sin(\omega_2)}$ and $\Delta_g \cos(\omega_2)$ due to the TM2 applied voltage. The components of $q(t)$ proportional to $\Delta g_{\sin(\omega_1)}$ and $\Delta g_{\sin(\omega_2)}$ are real signal, while any non-zero cosine components are noise in the measurement.

To obtain the charge time series components from the Δg data, two parallel methods are employed: heterodyne demodulation and least-squares fitting. These are two independent pipelines which arrive at equivalent charge time series, providing mutual verification. For supplemental information on these methods see Appendices A and B.

First, Δg was low-passed with cut-off frequency, $f_c = 15mHz$ and the applied voltages were low-passed with cut-off frequency, $f_c = 10mHz$. The data was then split so that each

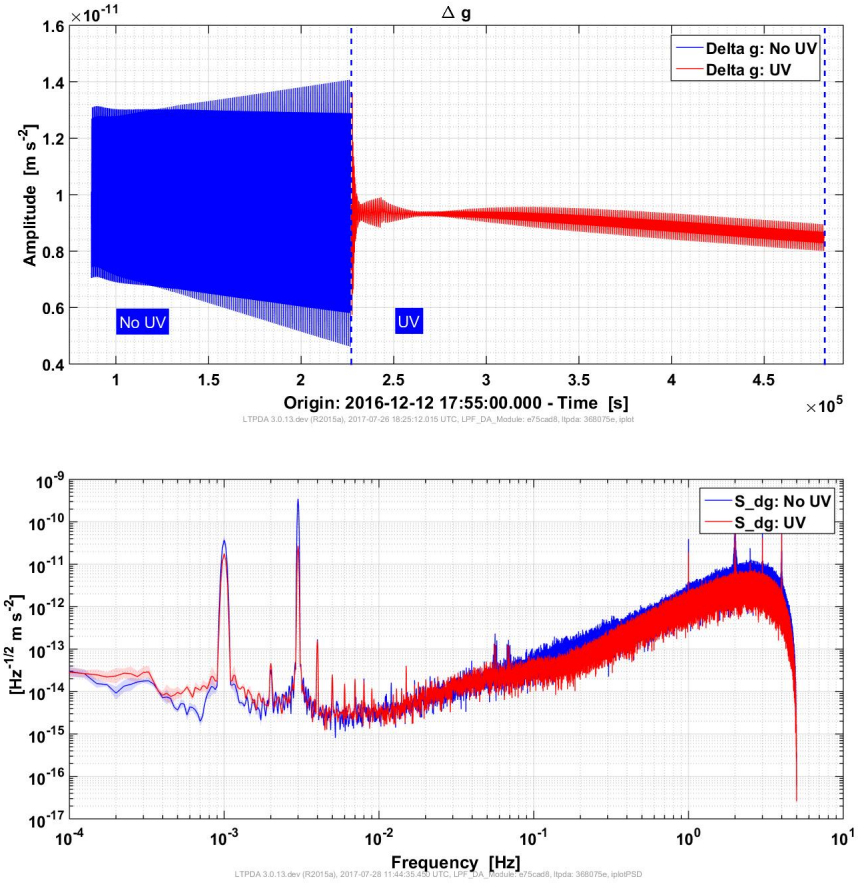

Figure 2: Top: Time series of Δg low passed with cutoff frequency, $f_c = 15mHz$. Bottom: ASD of Δg calculated using 40,000 second Blackman-Harris windows with 50% overlap. Blue: Δg during charging investigation. Red: Δg during initial and continuous UV discharge.

investigation could be analyzed separately. (See Table 1.

Heterodyne demodulation was calculated using the *stabilitydemod* function in LTPDA. Data was averaged over $1000s$ windows and the voltage applied to electrode x_1 was used as the phase reference. A 10-parameter fit was calculated using the *lscov* function in LTPDA. Fitting was performed with $2000s$ fitting windows. The window size was chosen so as to average out high frequency noise components that linger in a fit of shorter window lengths. Again the applied voltage, V_{x1} was used as the phase reference. A discussion comparing the two methods is given in the following section and in Appendix C.

4 Results

The section begins by discussing the differential acceleration in both time and frequency space. This is followed by a comparison of the parallel methods used to calculate the charge time series. We then present findings that characterize the differences in measurement noise between the TM charging and continuous discharge investigations. Finally we present an exponential fit of the charge time series under continuous UV discharge along with discussion of the physically meaningful fit parameters.

4.1 Differential Acceleration

The differential acceleration time-series is shown in Figure 2. Keeping in mind that Δg is related to $q(t)$ only by a constant, the general behavior of the charge is inferred from this plot. Charge build-up during the first investigation produces the cone shape seen in the first half of the figure. The red curve in the second half of the figure indicates that the charge initially decreases rapidly, corresponding to the time period in which the UV lamps were switched on to high power (see Table 1). Then Δg indicates that the charge began to slowly build up, crossing through zero, and finally settling towards an equilibrium value.

The power spectral density (PSD) of Δg was calculated during each investigation using the Welch method with 40,000s Blackman-Harris windows of 50% overlap. A window length of 40,000 seconds produces a PSD data point as low as .1mHz (see Figure 2). 50% window overlap means there is averaging in the PSD calculation. The error in PSD goes as $1/\sqrt{N_{win}}$; overlapping the windows gives a larger number of windows in the same time interval and thus less noise and a more accurate result. The particular method and parameters used for calculating the PSD were also chosen for consistency with previous LPF data analyses. Figure 2 shows the amplitude apectral density (ASD) of Δg. Peaks in each curve are clearly visible at $1mHz$ and $3mHz$, the injection frequencies. Roughly $\frac{1}{f}$ behavior is observed in the tail, below $1mHz$.

4.2 Charge Time Series

As previously mentioned, the charge time series, $q(t)$, was calculated using two independent pipelines: heterodyne demodulation and least-squares fitting. The two methods were compared and their results are plotted for both TM1 and TM2 in Figure 3. The most significant deviation between the two methods is seen in the quadrature component of $q(t)$ during the first investigation. Heterodyne demodulation produced a linear drift in $q_{\cos}$ that is not present in the same quantity when calculated by least-squares fitting. This drift is not physically meaningful as $q_{\cos}$ represents only the noise in the charge measurement. It is expected that this is indicative of some systematic error in the demodulation method. For this reason, all subsequent calculations presented in the following sections use the charge time series as obtained from least-squares fitting. Enlarged plots and further discussion of these methods are given in Appendix C for the interested reader.

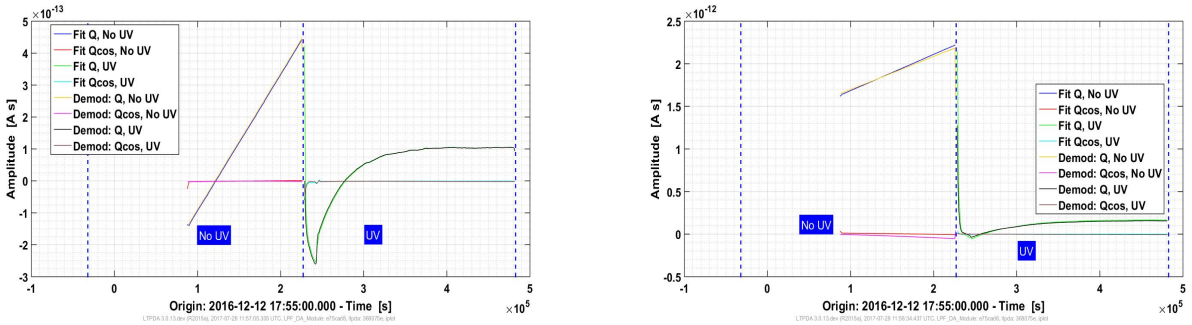

Figure 3: Left: TM1 Charge. Right: TM2 Charge. Results are presented as obtained from both heterodyne demodulation of Δg as well as a least-squares fit of Δg.

4.3 Measurement Noise

The PSD of each charge time-series was calculated, in the same way as $S_{\Delta g}$, using 40,000 second Blackman-Harris windows.

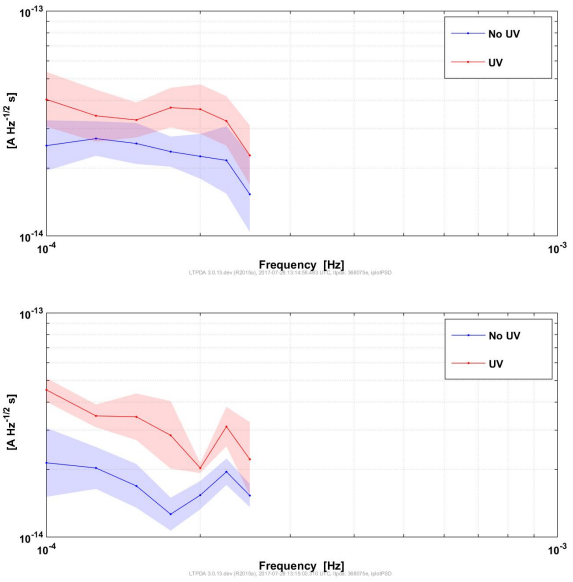

Figure 4: Top: TM1; Bottom: TM2. Blue: ASD of $q(t)$ from first investigation, during charge accumulation. Red: ASD of $q(t)$ from second investigation, during UV discharge.

S_q has a $1/f$ dependence in the low frequency band (shown scaled to ASD in Fig. 4). Fits of S_q to $1/f$ were calculated using LTPDA's *lscov* function and are shown in Figure 5. The fit slopes are presented in Table 3. The slope of the $1/f$ fit is greater during Investigation 2 for both TM1 and TM2. Based on an assumption of Poissonian noise in each TM, S_q scales with the event rate λ.

$$S_q = \frac{2e^2\lambda}{(2\pi f)^2} \tag{17}$$

The larger slopes during the UV discharge investigation (Figure 5, light blue) for both TM1 and TM2 indicate that the event rate increases during discharging. This would produce more noise in the measurement of charge during UV discharge as opposed to taking the measurement while charge is accumulating on the test mass. The event rates were calculated for both of TM1 and TM2 in each investigation using the value of S_q at $f = .1mHz$.

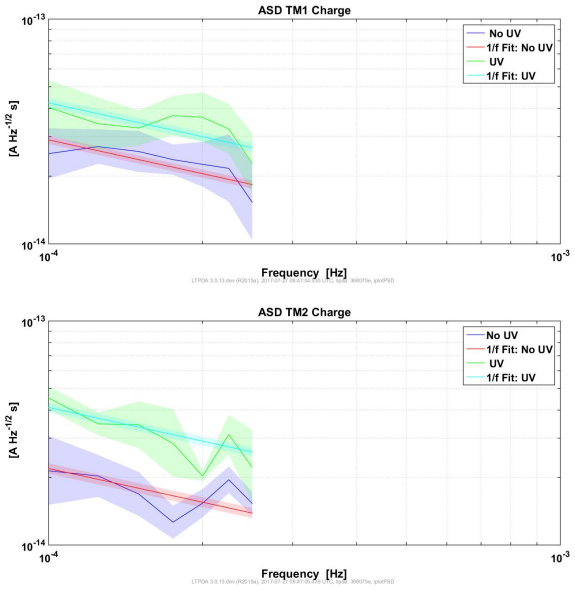

Figure 5: $1/f$ fits of ASD of $q(t)$. Top: TM1, Bottom: TM2.

$m\ [(A \cdot s)^2]$	**TM1**	**TM2**
No UV	$8.42 \cdot 10^{-32}$	$4.82 \cdot 10^{-32}$
UV	$1.79 \cdot 10^{-31}$	$1.69 \cdot 10^{-31}$

Table 3: Slopes of S_q fit to $1/f$. $S_q = m \cdot \frac{1}{f}$.

$\lambda\ [s^{-1}]$	**TM1**	**TM2**
No UV	$6.33 \cdot 10^5$	$3.26 \cdot 10^6$
UV	$1.35 \cdot 10^6$	$1.14 \cdot 10^7$
$\frac{\lambda_{UV}}{\lambda_{NoUV}}$	2.12	3.51

Table 4: Event rates for TM1 and TM2 during each investigation $[s^{-1}]$. The third row shows the ration of the event rate during UV illumination to the event rate without UV illumination.

The measurement noise in Δg was calculated from data during which no experiment took place. This is referred to as a noise-run and took place at the end of Decemeber, 2016. The noise

in Δg during such a period of time is taken as the lower-limit of measurement noise since it is present in the detector itself and not due to any experiment or applied conditions.

The ASD of Δg from the noise run is shown in Figure 6. In the mHz frequency range, $S_{\Delta g}^{1/2}$ is nearly white in frequency at a value of about $3fms^{-2}Hz^{-1/2}$. From this, we calculate error bars on Δg from the charge measurement experiment.

$$\delta(\Delta g) = \frac{\sqrt{2}S_{dg}^{1/2}}{\sqrt{T}} \tag{18}$$

where $T = 2\frac{1}{f_{mod}}$.

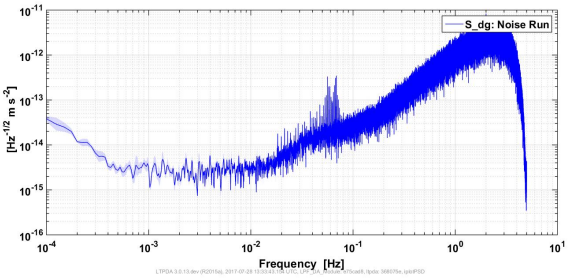

Figure 6: ASD of Δg calculated from noise-run: 2016-12-30 00:00 - 2016-12-31 00:00 UTC.

Recalling that Δg is simply related to $q(t)$ by the conversion factor,

$$\frac{dg}{dq} = \frac{4\left|\frac{dC}{dx}\right| V_{mod}}{mC_{tot}}$$

we calculate error bars on q_{TM1} and q_{TM2} as,

$$\delta q_{TM1} = \frac{\delta(\Delta g_1)}{|dg/dq|}$$
$$\delta q_{TM2} = \frac{\delta(\Delta g_2)}{|dg/dq|}$$

where δq_{TM1} and δq_{TM2} differ only in the value of f_{mod}. These errors are presented in Table 5.

	TM1	**TM2**
$\delta g\ [ms^{-2}]$	$9.42 \cdot 10^{-17}$	$1.63 \cdot 10^{-16}$
$\delta q[C]$	$5.33 \cdot 10^{-17}$	$9.24 \cdot 10^{-17}$

Table 5: Calculated errors in the differential acceleration and charge measurements of TM1 and TM2 with $f_{mod1} = 1mHz$, $f_{mod2} = 3mHz$

To compare the noise in the charge measurement between the two investigations the charge values with the previously calculated error bars were linearly detrended. Since $q(t)$ during the UV discharging investigation is exponential in nature, we first split the time series to consider only the last 50,000 seconds where $q(t)$ is approximately linear. For consistency, $q(t)$ during the first investigation is also split to an interval of 50,000 seconds before detrending. The results of this analysis are shown in Figure 7. Here the excess scatter of charge data corresponding to the UV discharging investigation is visible, indicating, as expected, more noise in this measurement.

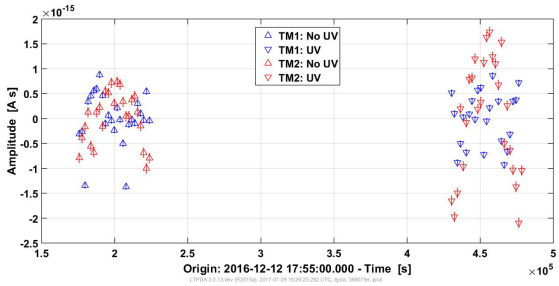

Figure 7: Detrended $q(t)$. Blue: TM1 charge; Red: TM2 charge; Upward triangles: charging investigation (no UV illumination); Downward triangles: continuous UV discharge investigation.

4.4 Exponential Fit

The charge-time series during the continuous discharge period of the second investiagtion were fit to a two-term exponential curve of the following form.

$$q(t) = ae^{bt} + ce^{dt}$$

The fit parameter d was set to 0 so that c represents the equilibrium charge value. We define,

$$q_{eq} = c$$

The charging time constant, τ is given by,

$$\tau = \frac{-1}{b}$$

We also rename the first parameter, $a = \Delta q$.

	TM1	**TM2**
$\Delta q\ [A \cdot s]$	$-4.523 \cdot 10^{-10}$	$-3.041 \cdot 10^{-11}$
$\tau\ [s]$	$3.33 \cdot 10^{4}$	$5.00 \cdot 10^{4}$
$q_{eq}\ [A \cdot s]$	$1.065 \cdot 10^{-13}$	$1.682 \cdot 10^{-13}$

Table 6: Exponential properties of TM charging under continuous UV illumination. Exponential fits take the form: $q(t) = \Delta q e^{-t/\tau} + q_{eq}$.

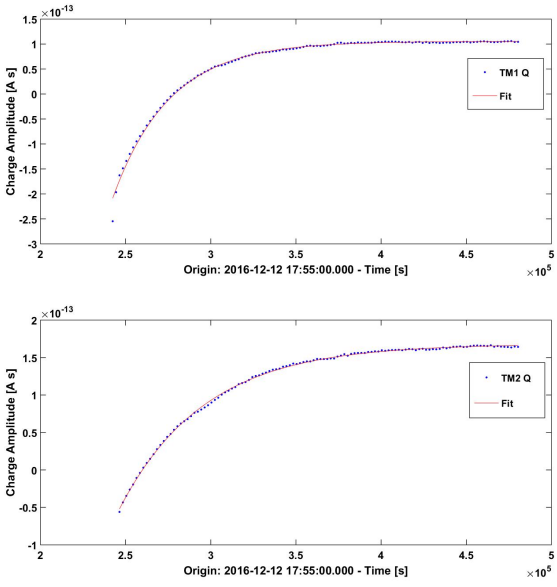

Figure 8: Exponential fit of the form $q(t) = ae^{bt} + c$ for TM1 charge (top), TM2 charge (bottom). Fits are calculated to 95% certainty using Matlab's built-in *fit* function.

5 Discussion

The results determine that, as expected, the continuous method of discharging test masses onboard LPF is inherently noisier than allowing the test masses to accumulate charge during science measurements. Although the net amount of charge on the test mass remains near neutral at the equilibrium value, there is significantly more movement of charge at all times. In addition to the movement of charge due to incident cosmic rays and solar particles UV discharging produces a current of charges moving between the electrode housing and the test mass. Reflection of the incident UV light within the electrode housing produces secondary currents in the opposite direction as the main discharging current. This is the source of the extra noise in the UV discharging method. There is a trade-off between the two methods. Continuous discharging allows the test masses to remain at a constant value near neutral although producing more noise in the measurement. This excess noise is indicated in the large amount of scatter in the detrended $q(t)$ plots.

Figures 2 and 3 show that the charge quickly decreases under the initial high-power UV light illumination. Under continuous UV illumination, the charge on the test mass will have an exponential nature in time. As the photoelectric effect from the UV light counteracts environmental charging the test mass charge trends toward an equilibrium. The value of q_{eq} differs between the two test masses; both values are reported in Table 5. The time constant τ determines how quickly the test mass reaches its q_{eq}. If some unexpected environmental factor perturbs the system, depositing an abnormal amount of charge on the test mass the time constant determines how long the test mass will take to return to equilibrium.

Under normal conditions, once the test mass reaches q_{eq}, the charge value stays nominally constant in time. This differs from the original scheme, in which the test mass charge builds up linearly in time, throughout science measurements. A constant charge value may be easier to model and account for in the LISA budget than a time-varying one.

6 Conclusion

LISA will be a ground-breaking experiment, detecting gravitational waves from a space-based observatory for the first time. The sensitivity required by LISA is such that we must be able to characterize every noise source in the detection band prior to LISA's launch. Test mass charging produces significant noise in the mHz frequency band. The expeccted method for mitigating the charge-induced force noise in LISA is by continuous low-power UV light illumination. The results presented here add a noise characterization and charge time-series model to the current understanding of the continuous UV discharging method.

7 Supplemental Information

Appendix A: Principles of Heterodyne Demodulation

Heterodyne Demodulation is a principle of signal analysis with widespread uses although being founded on fairly simple mathematical theory. It is used to decompose a waveform into an 'in-phase' and 'out-of-phase' component, which in real applications translate to signal and noise components. We start with any signal, which for convenience we will say is a simple sinusoid.

$$x(t) = A\sin(w_0 t) \tag{19}$$

Now, we can multiply our signal by both a sine and cosine.

$$x_{\sin}(t) = x(t)\cdot 2\sin(wt) \tag{20}$$

$$x_{\cos}(t) = x(t)\cdot 2\cos(wt) \tag{21}$$

Here, the factor of 2 is introduced for convenience which will become clear presently. We can now take a closer look at our sine and cosine components using a few simple trigonometric identities.

$$x_{\sin}(t) = A\cdot[\frac{\cos[(w_0-w)t]-\cos[(w_0+w)t}{2}]\cdot 2$$

$$= A[\cos[(w_0-w)t]-\cos[(w_0+w)t] \tag{22}$$

And similarly for the cosine component, we obtain,

$$x_{\cos}(t) = A[\sin[(w_0+w)t]+\sin[(w_0-w)t]] \tag{23}$$

Now, if the angular frequency, w_0, of the signal is known we can pick $w = w_0$ so that the above expressions for $x_{\sin}$ and $x_{\cos}$ become,

$$x_{\sin}(t) = A(1-\cos(2w_0 t)) \tag{24}$$

$$x_{\cos}(t) = A\sin(2w_0 t) \tag{25}$$

Assuming the signal is a real signal and exists over some long time interval, we can consider what happens to $x_{\sin}(t)$ and $x_{\cos}(t)$ over time. In other words, we take the time average of $x_{\sin}(t)$ and $x_{\cos}(t)$ over multiple periods, T of the signal.

$$\langle x_{\sin}(t)\rangle = \tfrac{1}{T}\int_0^{nT} A(1-\cos(2w_0 t)dt$$

$$= A$$

$$\langle x_{\cos}(t)\rangle = \tfrac{1}{T}\int_0^{nt} A\sin(2w_0 t)dt$$

$$= 0$$

Therefore, over time the in-phase component, $x_{\sin}(t)$ recovers the amplitude of our signal and the out-of-phase component, $x_{\cos}(t)$ drops out to 0.

Appendix B: Principles of Least-Squares Fitting

As was previously shown, the differential acceleration, Δg of the two test masses is related the the voltage applied on either test mass, as well as the charge, $q(t)$ present on the test masses. Therefore, Δg can be expressed as the sum of the contributions from an initial charge present on the test masses, the voltage applied to TM1, and the voltage applied to TM2. That is,

$$\Delta g = (\Delta g_{q_0}) + (\Delta g_{V_{TM1}}) + (\Delta g_{V_{TM2}})$$

More precisely, Δg is expressed as the sum of three base functions each with an unknown amplitude.

$$\begin{aligned}\Delta g = \Delta g_0 + [\Delta g_{s1}\sin(w_1 t) + \Delta g_{c1}\cos(w_1 t)] \\ + [\Delta g_{s2}\sin(w_2 t) + \Delta g_{c2}\cos(w_2 t)]\end{aligned}$$

Here, the sine and cosine terms come from the sinusoidal voltages applied to the test masses. This approximation can be made more accurate by expanding the terms as a Taylor polynomial to first order.

$$\begin{aligned}\Delta g = \left[\Delta g_0 + \frac{d\Delta g_0}{dt}t\right] + \\ (\Delta g_{s1} + \frac{d\Delta g_{s1}}{dt})\sin(w_1 t) + \\ (\Delta g_{c1} + \frac{d\Delta g_{c1}}{dt})\cos(w_1 t) + \\ (\Delta g_{s2} + \frac{d\Delta g_{s2}}{dt})\sin(w_2 t) + \\ (\Delta g_{c2} + \frac{d\Delta g_{c2}}{dt})\cos(w_2 t)\end{aligned}$$

Now, we have that Δg depends on ten independent base functions, each with an unknown amplitude. For brevity, we will henceforth denote each base function as χ_i and its corresponding amplitude by a_i,for $i = 1 : n$. Note that in this particular case, $n = 10$.

Let $X_j = \begin{pmatrix}\chi_1 & \chi_2 & \cdots & \chi_n\end{pmatrix}$ and $A = \begin{pmatrix}a_1 & a_2 & \cdots & a_n\end{pmatrix}$. Δg is not a continuous function, rather it is made up of a finite number, m, of data points. Therefore, we define m functions, $f(X_j) = X_j \cdot A$ so that Δg can be defined as,

$$\Delta g_j = f(X_j) + \eta \tag{26}$$

where η is an error in the approximation. This expression is expanded out for all of the m data points giving,

$$\begin{pmatrix}\Delta g_1 \\ \Delta g_2 \\ \vdots \\ \Delta g_m\end{pmatrix} = \begin{pmatrix}X_1 \\ X_2 \\ \vdots \\ X_m\end{pmatrix}\begin{pmatrix}a_1 \\ a_2 \\ \vdots \\ a_n\end{pmatrix} \tag{27}$$

$$\begin{pmatrix}\Delta g_1 \\ \Delta g_2 \\ \vdots \\ \Delta g_m\end{pmatrix} = \begin{pmatrix}\chi_{1,1} & \cdots & \chi_{1,n} \\ \chi_{2,1} & \cdots & \chi_{2,n} \\ \vdots & \ddots & \vdots \\ \chi_{m,1} & \cdots & \chi_{m,n}\end{pmatrix}\begin{pmatrix}a_1 \\ a_2 \\ \vdots \\ a_n\end{pmatrix} \tag{28}$$

$$\begin{pmatrix}\Delta g_1 \\ \Delta g_2 \\ \vdots \\ \Delta g_m\end{pmatrix} = \begin{pmatrix}a_1\chi_{1,1} + \cdots + a_n\chi_{1,n} \\ a_1\chi_{2,1} + \cdots + a_n\chi_{2,n} \\ \vdots \\ a_1\chi_{m,1} + \cdots a_n\chi_{m,n}\end{pmatrix} \tag{29}$$

The vector A can take on an infinite number of values. For a given m the method of least-squares fitting picks out the particular values of the a_i that minimize the error in Δg. We will call this vector $\mathscr{A}$. That is, when $A = \mathscr{A}$ we have that,

$$\sum_{i=1}^{n}(\Delta g_j - f(X_j))^2 = min. \tag{30}$$

$$[\Delta g_j - (a_1\chi_{j,1} + \cdots + a_n\chi_{j,n})]^2 = min. \tag{31}$$

Δg is fit over a number of intervals of some given length, each with m data points. For each interval, we obtain $\mathscr{A}_j$ for $j = 1 : m$. These m vectors are averaged to obtain a single $\mathscr{A}$ for each interval of the fit. It is obvious then that the shorter the interval, the better the fit that can be obtained.

Appendix C: Charge Calculation Method Comparison

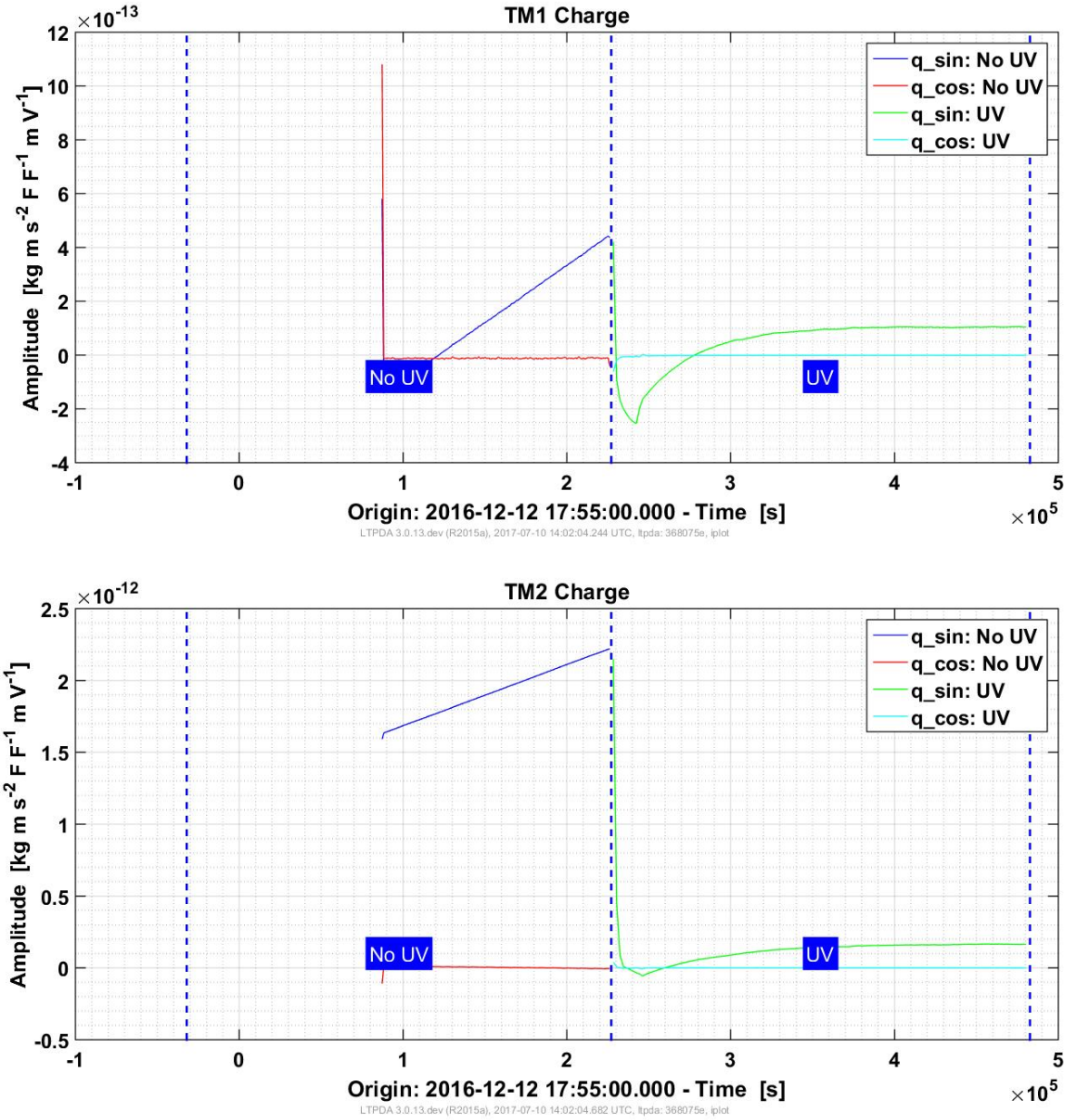

Figure 9: Enlarged plots of test mass charge time-series. Top: TM1, Bottom: TM2.

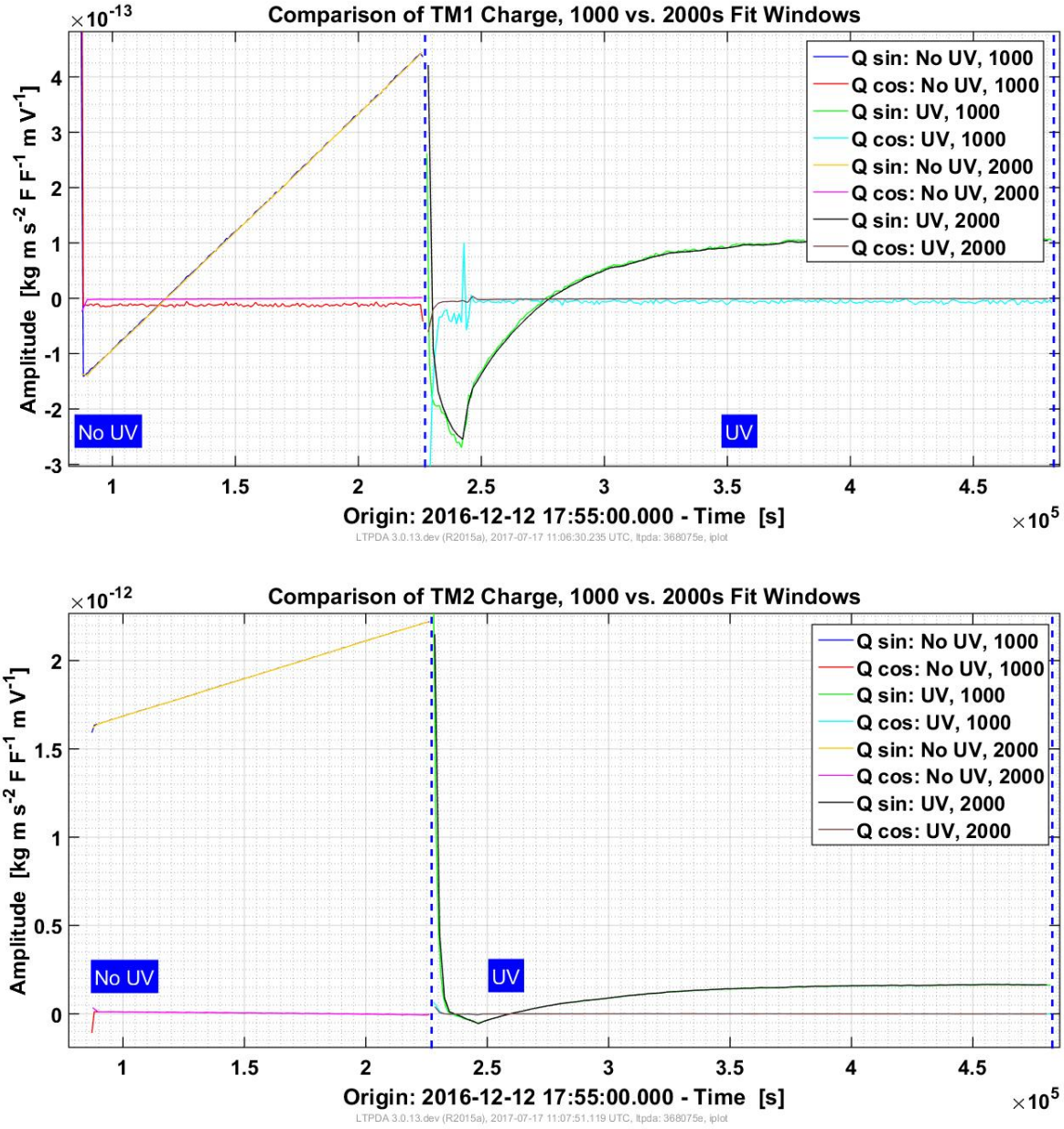

Figure 10: Charge measurement obtained from fits averaged over 1000 and 2000s windows. Top: TM1. Bottom: TM2. We note that for TM1 there is significant high-frequency noise in the 1000s fit. This noise averages out in the fit when using 2000s windows.

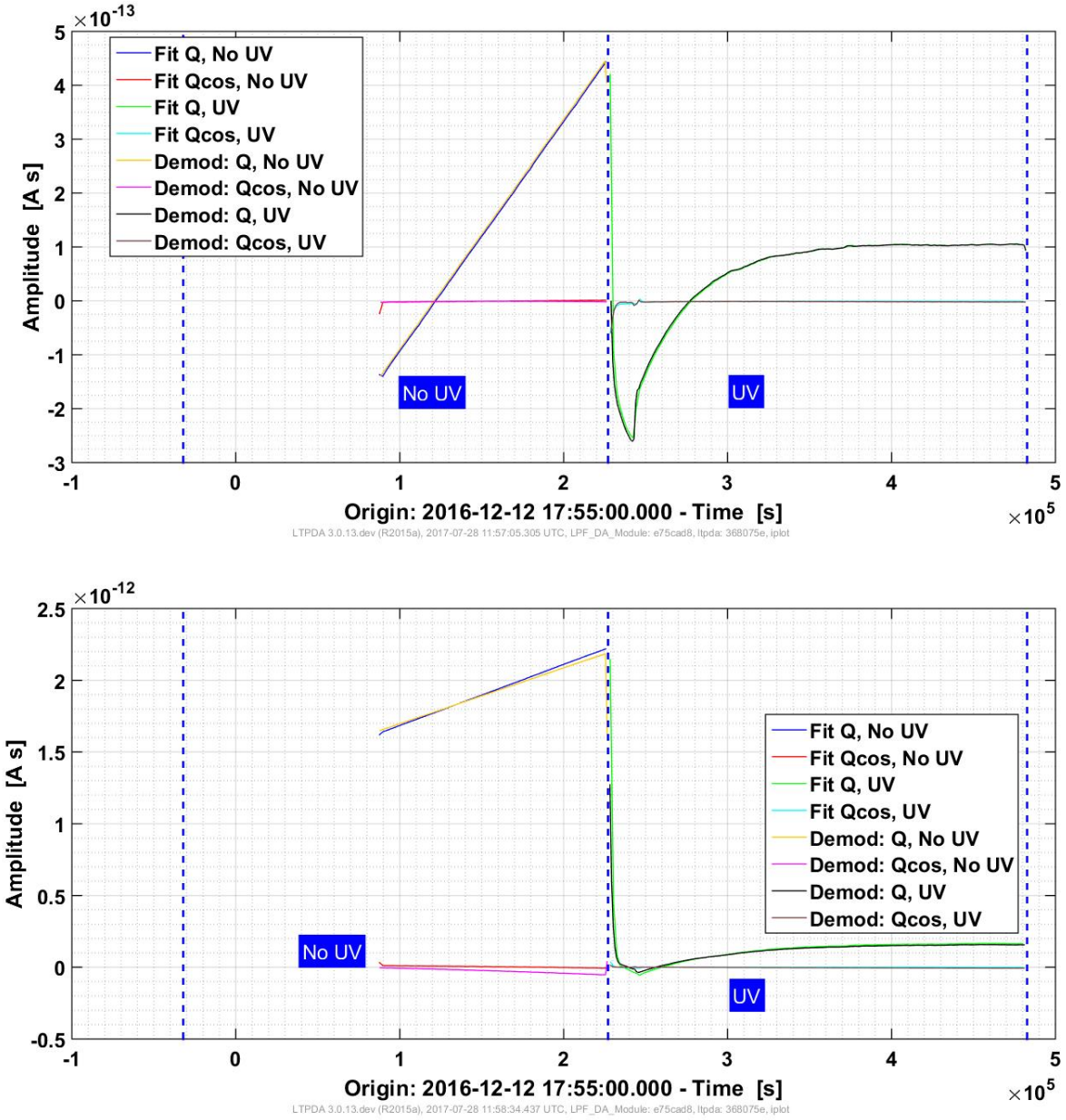

Figure 11: Comparison of charge measurement obtained from fit to charge measurement obtained from heterodyne demodulation. Top: TM1, Bottom: TM2. The fit was averaged over 2000s windows. We note the linear drift in the quadrature component of the charge from demodulation during Investigation 1. This is expected to be due to some unknown systematic error in the demodulation technique.

8 Acknowledgments

I would like to acknowledge the National Science Foundation, Dr. Mueller, and Dr. Whiting for making this program possible. I also want to thank Dr. Weber and Valerio for their patient help and genuine interest in my learning during the course of this summer.

9 References

1. B.P. Abbott et al. (2016). Observation of Gravitational Waves from a Binary Black Hole Merger. Phys. Rev. Lett. 116 (061102). 10.1103/PhysRevLett.116.061102

2. Armano M., Audley H., Auger G., Baird J., Binetruy P., Born M, ... Zweifel P. (2015). The LISA Pathfinder Mission. Journal of Physics: Conference Series, 610. doi:10.1088/1742-6596/610/1/012005.

3. Armano M., et al. (2016). Sub-Femto-g Free Fall for Space-Based Gravitational Wave Observatories: LISA Pathfinder Results. Physical Review Letters, 116(23). DOI: 10.1103/PhysRevLett.116.231101.

4. Armano M., et al. (2017). Charge-Induced Force Noise on Free-Falling Test Masses: Results from LISA Pathfinder. Physical Review Letters, 118 (17). DOI: 10.1103/PhysRevLett.118.171101

5. Hollington D., Baird J.T., Sumner T.J., and Wass, P. (2015). Characterising and Testing Deep UV LEDs for Use in Space Applications. Classical Quantum Gravity, 32(235020). DOI: https://doi.org/10.1088/0264-9381/32/23/235020.

6. Puecher, Anna. (2015-2016). LISA Pathfinder and test mass charging. University of Trento, Department of Physics.